

NASA CONTRACTOR
REPORT

NASA CR-179204

COMPUTATION OF TURBULENT FLOWS USING AN EXTENDED
k- ϵ TURBULENCE CLOSURE MODEL

By Y.-S. Chen and S.-W. Kim
Universities Space Research Association
Structures and Dynamics Laboratory
Science and Engineering Directorate

Interim Report

(NASA-CR-179204) COMPUTATION OF TURBULENT
FLOWS USING AN EXTENDED k-EPSILON TURBULENCE
CLOSURE MODEL Interim Report (Universities
Space Research Association) 27 p Avail:
NTIS HC A03/MF A01

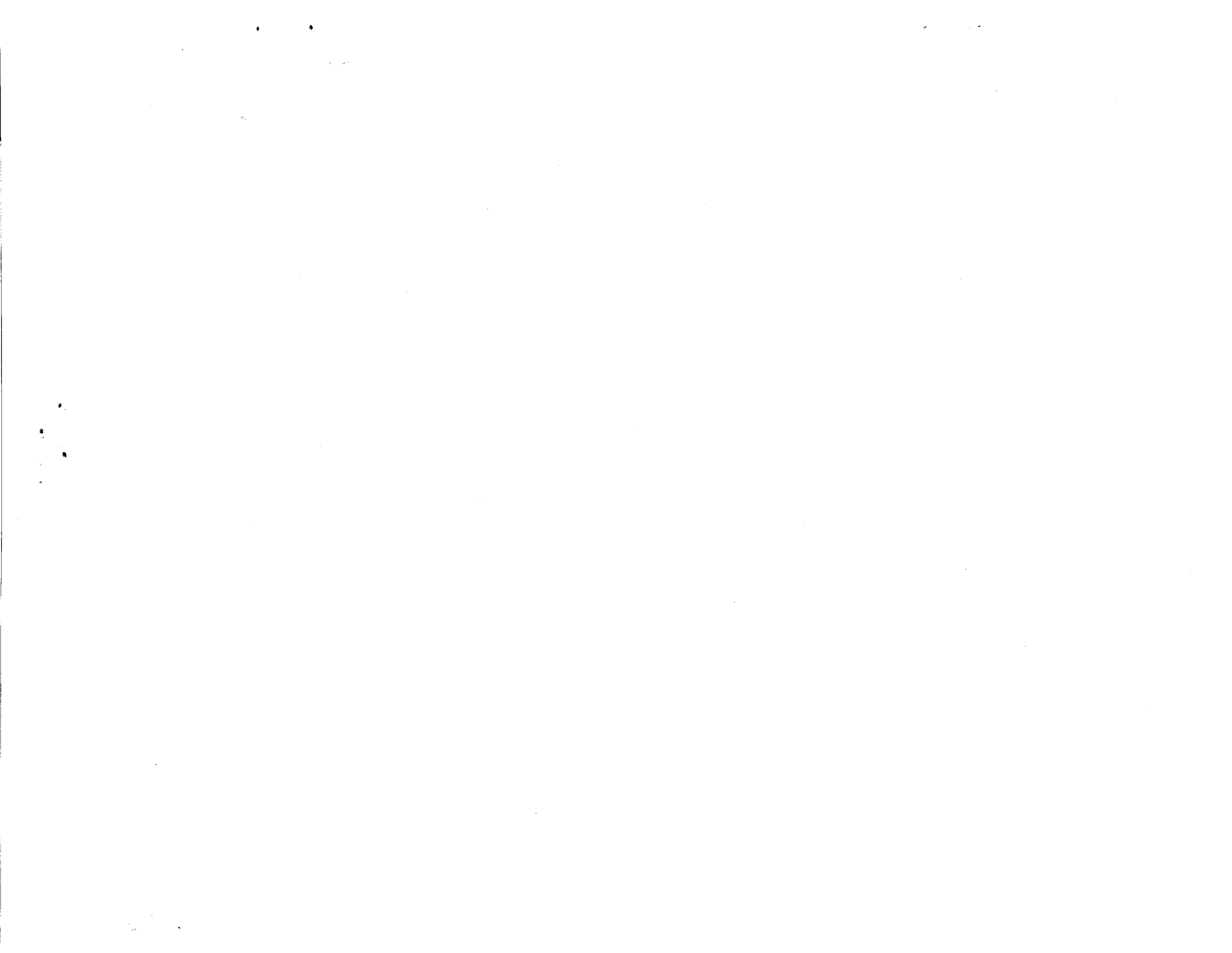
M88-11969

Unclas
0104481

CSCL 20D G3/34

October 1987

Prepared for
NASA-Marshall Space Flight Center
Marshall Space Flight Center, Alabama



| | | | | | |
|---|--|--|--|--|-------------------|
| 1. REPORT NO. NASA CR-179204 | | 2. GOVERNMENT ACCESSION NO. | | 3. RECIPIENT'S CATALOG NO. | |
| 4. TITLE AND SUBTITLE Computation of Turbulent Flows Using an Extended k- ϵ Turbulence Closure Model | | | | 5. REPORT DATE October 1987 | |
| | | | | 6. PERFORMING ORGANIZATION CODE | |
| 7. AUTHOR(S) Y.-S. Chen and *S.-W. Kim | | | | 8. PERFORMING ORGANIZATION REPORT # | |
| 9. PERFORMING ORGANIZATION NAME AND ADDRESS George C. Marshall Space Flight Center Marshall Space Flight Center, Alabama 35812 | | | | 10. WORK UNIT NO. | |
| | | | | 11. CONTRACT OR GRANT NO. NAS8-35918 | |
| 12. SPONSORING AGENCY NAME AND ADDRESS National Aeronautics and Space Administration Washington, D.C. 20546 | | | | 13. TYPE OF REPORT & PERIOD COVERED Contractor Report | |
| | | | | 14. SPONSORING AGENCY CODE | |
| 15. SUPPLEMENTARY NOTES *Universities Space Research Association Prepared by Fluid Dynamics Branch, Structures and Dynamics Laboratory, Science and Engineering Directorate. | | | | | |
| 16. ABSTRACT An extended k- ϵ turbulence model is proposed and tested in this paper with successful results. An improved transport equation for the rate of dissipation of the turbulent kinetic energy, ϵ , is proposed in the present study. The proposed model gives more effective response to the energy production rate than does the standard k- ϵ turbulence model. An extra time scale of the production range is included in the dissipation rate equation. This enables the present model to perform equally well for several turbulent flows with different characteristics, e.g. plane and axisymmetric jets, turbulent boundary layer flow, turbulent flow over a backward-facing step, and a confined turbulent swirling flow, etc. A second-order accurate finite difference boundary layer code and a nearly second-order accurate finite difference elliptic flow solver are used for the present numerical computations. | | | | | |
| 17. KEY WORDS Turbulence Boundary Layer Internal Flow Numerical Method | | | 18. DISTRIBUTION STATEMENT Unclassified/Unlimited | | |
| 19. SECURITY CLASSIF. (of this report) Unclassified | | 20. SECURITY CLASSIF. (of this page) Unclassified | | 21. NO. OF PAGES 25 | 22. PRICE NTIS |

ACKNOWLEDGMENT

This work was supported by the University Space Research Association under NASA Contract NAS8-35918.

TABLE OF CONTENTS

| | Page |
|---|------|
| INTRODUCTION | 1 |
| GOVERNING EQUATIONS | 2 |
| EXTENDED $k-\epsilon$ CLOSURE..... | 3 |
| NUMERICAL METHOD AND BOUNDARY CONDITIONS..... | 4 |
| RESULTS AND DISCUSSION | 5 |
| 1. Fully Developed Channel and Pipe Flows | 5 |
| 2. Submerged Jets | 6 |
| 3. Jets Exhausting into Moving Stream..... | 6 |
| 4. Flat Plate Turbulent Boundary Layer | 7 |
| 5. Backward-Facing Step Flow..... | 7 |
| 6. Confined Swirling Flow | 8 |
| CONCLUSIONS | 9 |
| REFERENCES | 10 |

LIST OF ILLUSTRATIONS

| Figure | Title | Page |
|--------|--|------|
| 1. | Fully developed channel and pipe turbulent flows | 13 |
| 2. | Plane turbulent jet exhausting into a moving stream | 14 |
| 3. | Plane turbulent jet exhausting into a moving stream | 15 |
| 4. | Axisymmetric turbulent jet exhausting into a moving stream..... | 16 |
| 5. | Wall shearing stress along a flat plate with zero pressure gradient..... | 16 |
| 6. | Flat plate turbulent boundary layer..... | 17 |
| 7. | Locus of flow reversal downstream of a backward-facing step | 18 |
| 8. | Static pressure coefficient distribution along the step side wall of a backward-facing step turbulent flow..... | 18 |
| 9. | Mean velocity and turbulent kinetic energy profiles downstream of a backward-facing step | 19 |
| 10. | Envelope of the central recirculation zone of a confined swirling turbulent flow | 20 |
| 11. | Center line axial velocity distribution of a confined swirling turbulent flow | 20 |

CONTRACTOR REPORT

COMPUTATION OF TURBULENT FLOWS USING AN EXTENDED k- ϵ TURBULENCE CLOSURE MODEL

INTRODUCTION

It is well known that, in the framework of isotropic or eddy viscosity turbulence closure modeling, good predictions of the mean and turbulent flow fields rely on reasonable descriptions of the turbulent length scale and velocity scale inside the flow field. The most widely used isotropic two-equation turbulence model is the standard k- ϵ model of Reference 1. This model, with standard model constants, has been applied over a wide range of turbulent flow problems [2,3,4]. In general, the standard k- ϵ model gives qualitative predictions for most turbulent flows, while the well-known plane jet and round jet anomaly is one of the typical problems that the standard k- ϵ model had failed to give consistent predictions as was described by Pope [5] and Hanjalić and Launder [6]. Although the spreading rate of plane jet was predicted correctly by the standard k- ϵ model, the spreading rate of round jet was over predicted by more than 30 percent. Also, for some bench-mark elliptic flow problems, such as a turbulent flow over a backward-facing step [4,7] and a turbulent confined swirling flow problem [8], etc., the standard k- ϵ model gives highly diffusive results. The reattachment length of the recirculation region of the backward-facing step flow, for instance, was measured to be around 7.2 step heights. However, the consensus prediction of the reattachment length using the standard k- ϵ model was reported to be around 5.2 step heights [7].

The inconsistency of the standard k- ϵ model is very often attributed to the dissipation rate equation which is highly empirical in nature. Improvement of the model performance is usually achieved by modifying the dissipation rate equation. In References 5 and 6, extra irrotational strains are added to the production term of the dissipation rate equation. With these modifications, some improvements in the generality of the k- ϵ model have been demonstrated [9,10]. For internal recirculating flow problems, many implementations for the k- ϵ model have been proposed by employing the so-called Richardson number correction for the ϵ -equation [11,12]. Although some improved predictions for certain types of elliptic flow problems have been reported using the Richardson number corrections, they were found to be problem dependent in nature [11,12].

In the present paper, a similar but more general approach is taken by adding a second time scale of the production range of turbulence kinetic energy spectrum to the dissipation rate equation. This extra time scale enables the energy transfer mechanism of the turbulence model to respond to the mean strain more effectively. The present modification results in one extra term along with one extra modeling constant added to the standard k- ϵ model. The new set of model constants are tuned based on the experimental data of homogeneous turbulence decay with or without mean strain imposed [13,14,15], a near wall boundary conditions analysis and numerical optimization.

Numerical examples included in the present paper involve fully developed turbulent channel and pipe flows [16,17], turbulent free-shear flows [18,19,20,21], flat plate turbulent boundary layer [22], turbulent flow over a backward-facing step [4,7]

and a confined turbulent swirling flow [8]. This wide variety of example problems is included to assess the performance and generality of the present extended $k-\epsilon$ turbulence model. For numerical computations, a second-order accurate finite difference boundary layer code was used for boundary layer type flow problems and a nearly second-order accurate finite difference elliptic flow solver was used for the internal turbulent flow problems in the present study. The boundary layer code employs stream-wise marching technique using a second-order backward differencing scheme. In the transverse direction, a second-order upwind differencing scheme is used for the convection terms and a central differencing scheme is used for the diffusion terms. In the elliptic flow solver, the diffusion terms of the governing equations are discretized by using a central differencing scheme and the convection terms are discretized by using a second-order upwind differencing scheme [23,24]. Favorable results of many other example problems using the present $k-\epsilon$ turbulence model and a rigorous and accurate finite element boundary layer code can be found in Reference 25. Results of Reference 25 reflect and confirm the consistency of the present turbulence model using both finite difference and finite element methods.

GOVERNING EQUATIONS

For steady incompressible turbulent flows, the flow field can be characterized by conservation laws. These are the continuity equation and the Navier-Stokes (or momentum) equations. With the commonly used Reynolds decomposition and averaging procedure, the system of governing equations for turbulent flow field can be written in the following form [26].

$$(\rho u)_x + (\rho v)_y = 0 \quad (1)$$

$$\rho u u_x + \rho v u_y - (\mu_e u_x)_x - (\mu_e u_y)_y = -p_x + (\mu_e)_x u_x + (\mu_e)_y v_x \quad (2a)$$

$$\rho u v_x + \rho v v_y - (\mu_e v_x)_x - (\mu_e v_y)_y = -p_y + (\mu_e)_x u_y + (\mu_e)_y v_y \quad (2b)$$

$$\mu_e = \mu + \mu_t$$

where u and v are velocity vectors in x - and y -coordinate directions, respectively, μ and ρ represent the fluid viscosity and density, respectively, and p denotes the static pressure. The above governing equations can be simplified for boundary layer type flows [27]. In the above equations, the Boussinesq assumption has been used to relate the Reynolds stresses to the mean strains through the turbulent viscosity, μ_t . The turbulent eddy viscosity is then related to the turbulence length scale, l_t , and the turbulence velocity scale, u_t , which can be expressed in terms of other turbulence quantities, namely the turbulent kinetic energy, k , and its dissipation rate, ϵ . That is,

$$\mu_t = \rho l_t u_t \quad ; \quad l_t = C_\mu k^{3/2}/\epsilon \quad ; \quad u_t = k^{1/2} \quad (2c)$$

where C_μ is usually taken as a constant, $C_\mu \cong 0.09$. Although previous investigations [28,29,30] have suggested that C_μ should be a function of flow field quantities, modification of C_μ will not be considered here. Effects of C_μ function on the performance of turbulence model can be found in References 25 and 30. The turbulence quantities, k and ϵ , are provided by employing an extended k - ϵ turbulence closure model which is described in the following section.

EXTENDED k - ϵ CLOSURE

For the closure of the governing equations, the widely used two-equation k - ϵ turbulence modeling approach is employed in the present study. The transport equation of the turbulent kinetic energy can be written as [1]:

$$\rho u k_x + \rho v k_y - [(\mu_t/\sigma_k) k_x]_x - [(\mu_t/\sigma_k) k_y]_y = \rho(P_r - \epsilon) \quad (3)$$

where P_r and ϵ represent the production rate and the dissipation rate of the turbulent kinetic energy, k , respectively, and σ_k is a modeling constant. The production rate is related to the mean strain of the velocity field through the Boussinesq assumption. That is,

$$P_r = (\mu_t/\rho)[(u_y + v_x)^2 + 2(u_x^2 + v_y^2)] .$$

For boundary layer type flows, the production rate can be simplified to be:

$$P_r = (\mu_t/\rho) u_y^2 .$$

However, for rapidly evolving flow fields (e.g., plane jet or round jet exhausting into a still air), it is more appropriate to retain the full production term to have better representation of the energy generation rate.

For the dissipation rate equation, two time scales are included to allow the dissipation rate to respond to the mean strain more effectively than that of the standard k - ϵ model. This is the major improvement of the present k - ϵ model for complex turbulent flow problems. The time scales included in the present model are: the production range time scale, k/P_r , and the dissipation rate time scale, k/ϵ . The final expression of the dissipation rate transport equation is given as:

$$\rho u \epsilon_x + \rho v \epsilon_y - [(\mu_t/\sigma_\epsilon) \epsilon_x]_x - [(\mu_t/\sigma_\epsilon) \epsilon_y]_y = \rho(C_1 P_r \epsilon/k - C_2 \epsilon^2/k + C_3 P_r^2/k) . \quad (4)$$

The last term of equation (4) represents the energy transfer rate from large scale turbulence to small scale turbulence controlled by the production range time scale and the dissipation rate time scale. The net effect of the present energy transfer function enhances the development of ϵ when the mean strain is strong, or large production rate, and the generation of ϵ is suppressed when the mean strain is weak, or small production rate. Consequently, as the model constants are carefully tuned, the present formulation enables the dissipation rate to respond to the mean flow field more rapidly so as to control the development of the turbulent kinetic energy more effectively.

To determine the model constants, C_1 , C_2 , and C_3 , experimental data of the decay of homogeneous turbulent flows, with or without mean strains [13,14,15], and a simplified near wall analysis [25] are used to decide the feasible range of these constants. Numerical optimization is then employed to anchor the final model constants by matching the predictions to the measured data of several simple turbulent flows, i.e., fully developed turbulent channel and pipe flows and turbulent plane jet. For the rest of the two model constants, σ_k and σ_ϵ , two simple physical arguments are imposed to set up two criteria for determining these two constants. First, any turbulence model must satisfy the realizability [31], especially near the edge of boundary layers, such that the dissipation rate would be vanishing, in the direction away from the boundary layer, at a rate faster than that of the turbulent kinetic energy. This requires that σ_k is smaller than σ_ϵ . Secondly, by observing many data of boundary type turbulent flows [18,19,20,21,22], it is obvious that the boundary edges of the turbulent kinetic energy extend much wider (about 10 percent wider) than that of the mean velocity profiles. This implies that it is proper to have σ_k less than unity. The final numbers of these model constants are:

$$\sigma_k = 0.75 \quad ; \quad \sigma_\epsilon = 1.15 \quad ; \quad C_1 = 1.15 \quad ; \quad C_2 = 1.9 \quad ; \quad C_3 = 0.25 \quad .$$

Detailed descriptions about the determination of these model constants can be found in Reference 25.

NUMERICAL METHOD AND BOUNDARY CONDITIONS

A finite difference marching procedure is employed in the present study to carry out the computations of boundary layer type turbulent flow problems. The present finite difference method includes a second order central difference approximation for the cross-stream diffusion terms. For the cross-stream convection terms, a second order upwind differencing scheme is employed. In the stream-wise (or marching) direction, a second order backward (or upwind) differencing scheme is used to provide a fully implicit boundary layer marching procedure. The whole numerical scheme has the accuracy of second order. Uniform grid systems in the longitudinal and transverse directions are employed to cover the entire physical domain. This requires that the initial computational domain in the transverse direction extend outward several boundary layer thicknesses.

At the initial data station, experimental measurements of the mean velocity profile and the turbulent kinetic energy distribution are employed. Measurements of

Reynolds stress are used to generate the initial dissipation rate distribution through the Boussinesq assumption and equation (2c). Along the free stream boundary and the center line of jet flows, zero normal gradients (or vanishing flux) boundary conditions are imposed. Near the solid wall boundary, the commonly used wall function approach [2] is employed to provide boundary conditions for the velocity and turbulence quantities. This wall function approach is based on the assumptions of a logarithmic wall law velocity profile and a near wall turbulent kinetic energy equilibrium condition. Although these assumptions are not valid for boundary layers subject to stream-wise curvature effects, strong adverse pressure gradient or flow separation, the choice of the approach for solid wall boundary conditions is, to the best knowledge of the authors, due to the lack of a better and more general alternative at the present time.

For elliptic flow problems, a 2-dimensional finite difference elliptic flow solver is employed [23,24]. In this elliptic flow solver, central differencing is used to approximate the diffusion terms. For the convection terms, a second order upwind differencing scheme is implemented in the basic solver of References 23 and 24 to provide numerical stability and retain numerical accuracy close to second order. The pressure field is obtained by employing the SIMPLE-C algorithm of Reference 32, which corrects the pressure and velocity fields successively until the conservation of mass is satisfied throughout the entire computational domain. The convergence criterion of the present elliptic flow solver requires the sum of the maximum correction of the velocity and pressure between two successive iterations to be less than 10^{-4} .

At the entrance of the computational domain, inlet boundary conditions are specified. At the exit, zero gradient boundary conditions are imposed. Near the solid wall, the conventional wall function approach is used [2]. For axisymmetric flow problems, symmetric boundary conditions are imposed along the axis.

RESULTS AND DISCUSSION

In order to assess the performance of the present turbulence model, several boundary layer and elliptic turbulent flow problems were tested in the present study. These flow problems include: fully developed turbulent channel and pipe flows [16,17]; turbulent plane jet and round jet [18,19,20,21]; a flat plate turbulent boundary layer flow [22]; an internal turbulent recirculating flow over a backward facing step [4,7]; and a confined turbulent swirling flow [8]. Results of the computation of the above flow problems are discussed in detail below.

1. Fully Developed Channel and Pipe Flows

For these test cases, experimental data given by Laufer [16,17] were used for data comparisons. The Reynolds numbers of the selected cases of the fully developed channel and pipe flows were 61,600 and 200,000, respectively. The center line velocity of the channel and pipe flows were 7.05 m per sec and 30.05 m per sec, respectively. For fully developed flow problems, the boundary layer equations can be further simplified to be a system of ordinary differential equations. Symmetric boundary conditions were specified at the channel or pipe center line. Near the wall boundary, experimental data of the mean velocity and the turbulent kinetic energy were specified as fixed boundary conditions which were intended to avoid errors arising from the use of wall function approximations. The near wall dissipation rate was estimated

by using the mixing length approximation. The longitudinal pressure gradient was given by the experimental data. Fifty grids were used for the computations of these cases.

Figures 1(a) and 1(b) show comparisons of the predicted and the measured mean velocity and turbulence quantities for the channel and pipe flows, respectively. It is clear in Figure 1 that the present turbulence model gives satisfactory predictions for these test cases. The standard $k-\epsilon$ model gives almost the same predictions.

2. Submerged Jets

Two submerged-jet, i.e., jet exhausting into a still air environment, problems were studied which included a submerged plane jet [18] and a submerged round jet [19]. Spreading rate of the jet half width, $dy_{1/2}/dx$, is of major concern here. Experimentally, the submerged jet can reach a constant spreading rate within $30d$ downstream of the jet exit, where d stands for the jet nozzle width or diameter. The experimental spreading rates of the submerged plane jet and round jet were found to be 0.11 and 0.098, respectively.

In the present study, computations of the submerged jets started from $10d$ downstream of the jet exit. The initial velocity and turbulent kinetic energy profiles were generated using the similarity profiles. The initial data for the dissipation rate were then estimated from the Reynolds stress distribution through the Boussinesq assumption and equation (2c). Computational domain in the transverse direction extended outward 10 times the initial jet width to allow marching to $40d$ downstream. Due to the rapidly evolving velocity field, the full production expression was used in the present turbulence model to give a better representation of the non-boundary-layer character of the flow field. This kind of implementation was found to be only necessary for the submerged jet problems since velocity gradients in the stream-wise direction are not negligible.

The spreading rates of the submerged jets were then calculated from the solutions of the marching procedure. The results show that the computed spreading rates of the submerged plane and round jets are 0.111 and 0.108, respectively. Using the same form of production term, the standard $k-\epsilon$ turbulence model produced spreading rates of 0.117 and 0.119 for the plane and round jets, respectively. With the simplified production term (as commonly used), the standard $k-\epsilon$ model gave spreading rates of 0.11 and 0.125 for the two jets, respectively. From these results, it is apparent that the effect of the full production term treatment is significant for rapidly developing flow fields.

3. Jets Exhausting into Moving Stream

Two co-flowing jet problems were included in the present study. These two cases correspond to the experimental investigations of Bradbury [20], for a plane jet exhausting into a moving stream of speed 7.344 m/s, and of Antonia and Bilger [21], for an axisymmetric jet exhausting into a moving stream of speed 30.5 m/s. For the plane jet problem, the jet velocity at the exit of a jet slot with width, $d = 0.009525$ m, was 45.9 m/s. Numerical computation was started from $10d$ downstream of the jet exit, where measured data of mean velocity and turbulence intensities distributions were given. Solutions were obtained by using the present marching procedure from $x = 10d$ to $x = 70d$. Ninety-one grids in the transverse direction were used in the marching procedure. Figure 2 illustrates comparisons of the measured and the

predicted decay of the center line velocity, u_c , and growth of the jet half width, $y_{1/2}$. Detailed comparisons of the mean velocity profiles and the distributions of turbulence quantities are shown in Figure 3 for $x = 40d$ and $x = 68d$. It is clear from these results that the present turbulence model reproduces the experimental data very well except slight discrepancies in the turbulent kinetic energy profile at $x = 68d$.

For the case of round jet, the jet exit velocity out of a nozzle with diameter, $d = 0.00528$ m, was 137 m/s. The same marching procedure was used for this problem. Since only self-similar profile data were given in Reference 21, the initial data were generated from the similarity profiles which do not resemble the real test conditions. Therefore, only the comparisons of the self-similar profiles are presented in Figure 4. Numerically, self-similar profiles were produced using results after $50d$ downstream of the initial data plane. Figure 4 shows that the present turbulence model also gives good predictions for this round jet problem.

4. Flat Plate Turbulent Boundary Layer

In this example, a turbulent boundary layer developing along a flat plate with zero pressure gradient was examined. The experimental case of Wieghardt [22] was simulated. The free stream velocity was 33 m/s. The initial data plane was located at $x = 0.94$ m and the marching procedure was performed up to $x = 5.0$ m. Ninety-one grids in the transverse direction were used in the marching procedure. Figure 5 shows the comparisons of wall shearing stress distributions using the standard $k-\epsilon$ model and the present extended $k-\epsilon$ model. It can be seen from Figure 5 that the standard $k-\epsilon$ model over-predicts the wall shearing stress by about 5 percent while the present turbulence model under-predicts the wall shearing stress by about the same percentage. Figure 6 illustrates the comparisons of mean velocity profiles, turbulent kinetic energy profiles and Reynolds stress distributions at two stations, i.e., $x = 2.887$ m and $x = 4.987$ m. It is clear in Figure 6 that the mean velocity profiles are well predicted by the present turbulence model while discrepancies in turbulence quantities are apparent. This is mainly attributed to the inadequacy of the wall boundary conditions for k and ϵ using the conventional wall function approach [2] which gives low turbulent kinetic energy at the wall function point. Similar results were obtained using the standard $k-\epsilon$ turbulence model. Better wall boundary conditions may improve the predictions of the turbulence quantities in both models.

5. Backward-Facing Step Flow

One of the standard test cases of complex elliptic turbulent flow presented in the Stanford Conference [4] was a confined turbulent recirculating flow over a backward-facing step [7]. The experimental configuration contained a straight channel followed by a sudden expansion with 2:3 expansion ratio. The inlet flow velocity was about 18 m/s. The measured size of the separation region (reattachment length) caused by the sudden expansion was around 7.2 step heights. The computation of the reattachment length of this problem has been used extensively for assessing the performance of turbulence models [4].

In the present study, the computational domain extended 6 step heights upstream of the expansion plane and extended 30 step heights downstream of the expansion plane to enable the application of zero gradient exit boundary conditions. At the flow inlet, uniform velocity and turbulent kinetic energy profiles were specified. Inlet boundary condition of the dissipation rate was then estimated by assuming a

constant mixing length equivalent to 0.03 times the inlet channel width. Near solid wall boundaries, the conventional wall function approach was employed to provide boundary conditions for the momentum equations and the turbulence model. A 51 by 41 grid system was used for this case. This grid size yields grid independent solutions in which the difference in the reattachment length using grid sizes of 41 by 35 and 51 by 41 was less than 1 percent. The standard $k-\epsilon$ model and the present $k-\epsilon$ model were used for the current test case.

Figure 7 shows the comparisons of the locus of flow reversal (where the longitudinal velocity component, u , changes sign). It is clear that the present turbulence model gives much better predictions than the standard $k-\epsilon$ model. The present turbulence model predicts a reattachment length of 7.0 step heights while the standard $k-\epsilon$ model gives only 5.2 step heights. Figure 8 illustrates the comparisons of wall static pressure distributions along the step side wall. Good agreement between the present model predictions and the measured data is shown clearly in Figure 8 while apparent discrepancies are revealed for the standard $k-\epsilon$ model predictions. Figures 9(a) and 9(b) show detailed comparisons of the mean velocity profiles and the distributions of the turbulent kinetic energy downstream of the step. Again, improvements of the present $k-\epsilon$ model over the standard one are illustrated in the region near reattachment. It can be seen from Figure 9(b) that the turbulent kinetic energy overshoot phenomenon downstream of the expansion plane of the standard $k-\epsilon$ model is suppressed effectively by the present turbulence model which contains a more effective energy transfer function in the ϵ -equation, equation (4), see $x/h = 2.33$.

6. Confined Swirling Flow

In the present study, a confined turbulent swirling flow problem investigated experimentally by Roback and Johnson [8] was solved numerically. Several numerical studies of this flow using the standard $k-\epsilon$ turbulence model have been reported [32,33,34]. Experimentally, the swirling flow channel consisted of two coaxial inlet pipes with the swirling guide vanes installed between the inner and outer pipes. The inner and outer pipes had radii of 12.5 mm and 29.5 mm, respectively. The inlet channel was followed by a sudden pipe expansion with expansion ratio around 1:2. The radius of the downstream pipe, R_o , was 61 mm. The inlet swirling velocity generated by the swirling guide vane created a central recirculation zone along the pipe center line downstream of the expansion plane. This central recirculation zone was accompanied by a corner recirculation region downstream of the step.

In order to avoid geometrical and flow complexities upstream of the expansion plane, where a three-dimensional flow field was expected and detailed experimental data were not available, the present numerical computation employed the first data plane, which is 5 mm downstream of the expansion plane, as the inlet boundary where detailed experimental data were provided [8]. The exit boundary was located 1800 mm downstream of the expansion plane. A grid size of 51 by 41 was used for this test case. More grids were clustered near the inlet where rapid flow development is expected. The conventional wall function approach was again used for near wall boundary conditions. A converged solution was obtained in 1500 iterations due to the use of a second order upwind differencing scheme for the convection terms.

Computed results of the sizes of the central recirculation zones from the use of the present $k-\epsilon$ model and the standard $k-\epsilon$ model are compared with the measured data illustrated in Figure 10. Comparisons of the development of the center line velocity are presented in Figure 11. It is clear in Figures 10 and 11 that the present turbulence model predicts much better results than that of the standard $k-\epsilon$ model.

Figure 12 gives a detailed comparison of the radial distribution of the axial velocity at $x = 25$ mm. Again, the present turbulence model represents the measured data much better. Also, results predicted by the standard $k-\epsilon$ model are similar to those reported previously in References 32, 33, and 34.

CONCLUSIONS

In the present paper, an extended $k-\epsilon$ turbulence model has been proposed and tested for a wide variety of turbulent flow problems. An extra time scale has been introduced in the construction of the transport equation of the rate of dissipation of the turbulent kinetic energy. This results in an energy transfer function which has been found to be more effective than that of the standard $k-\epsilon$ turbulence model. Numerical tests of example problems including simple boundary type turbulent flows and complex internal turbulent recirculating flows have demonstrated that the present model is more general than the standard $k-\epsilon$ model. For simple boundary type turbulent flows, the present model gives similar results predicted by the standard $k-\epsilon$ model. However, for complex elliptic turbulent flow problems, which involve rapid changes of turbulent kinetic energy production and dissipation rates, the present extended $k-\epsilon$ has been shown to give much better results than the standard $k-\epsilon$ model. This is mainly attributed to the energy transfer function introduced in the dissipation rate equation which enables the development of the field of the dissipation rate to suppress the overshoot phenomenon of the turbulent kinetic energy, as revealed by the standard $k-\epsilon$ model, when the mean shear is strong.

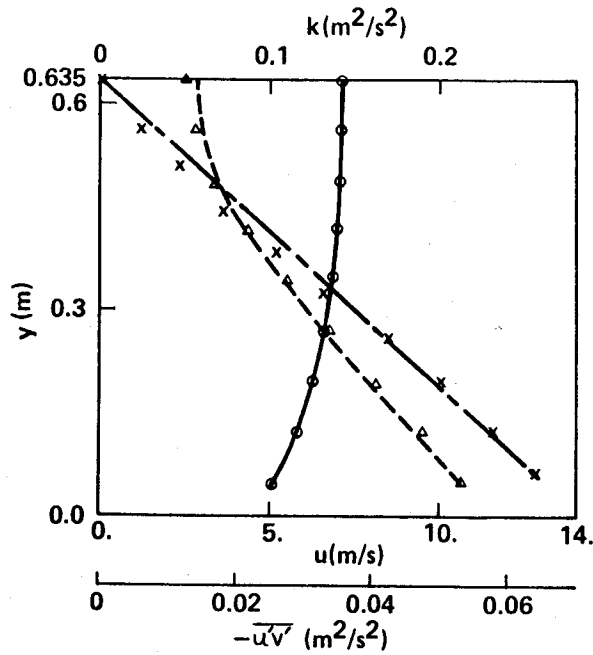
Applications of the present model to other complex turbulent flow problems, e.g., turbulent flows inside strongly curved ducts, turbulent flows inside turbomachinery passages, time dependent turbulent flow problems, etc., are planned for future study. This will give a better assessment of the generality of present turbulence model.

REFERENCES

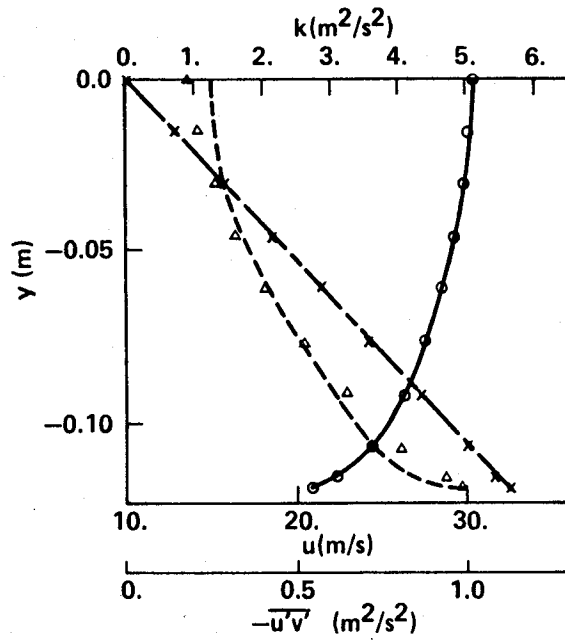
1. Launder, B. E., and Spalding, D. B.: Mathematical Models of Turbulence. Academic Press, London, 1972.
2. Launder, B. E., and Spalding, D. B.: The Numerical Computation of Turbulent Flows. *Comp. Meth. Appl. Mech. Engr.*, Vol. 3, 1974, pp. 269-289.
3. Launder, B. E., Morse, A., Rodi, W., and Spalding, D. B.: Prediction of Free Shear Flows - A Comparison of the Performance of Six Turbulence Models. NASA SP-321, July 1972.
4. Kline, S. J., Cantwell, B. J., and Lilley, G. M. (Ed.): The 1980-1981 AFOSR-HTTM-Stanford Conference on Complex Turbulent Flows. Stanford University, I, II, and III.
5. Pope, S. B.: An Explanation of the Turbulent Round-Jet/Plane-Jet Anomaly. *J. of AIAA*, Vol. 16, 1978, pp. 279-281.
6. Hanjalic, K., and Launder, B. E.: Sensitizing of the Dissipation Equation to Irrotational Strains. *Transactions of ASME*, Vol. 102, 1980, pp. 34-40.
7. Kim, J. J.: Investigation of Separation and Reattachment of a Turbulent Shear Layer: Flow Over a Backward Facing Step. Ph.D. Thesis, Stanford University, 1978.
8. Roback, R., and Johnson, B. V.: Mass and Momentum Turbulent Transport Experiments with Confined Swirling Coaxial Jets. NASA CR-168252, August 1983.
9. Wood, P. E., and Chen, C. P.: Turbulence Model Predictions of the Radial Jet - A Comparison of the $k-\epsilon$ Models. *The Canadian J. Chemical Engr.*, Vol. 63, pp. 177-182, April 1982.
10. Rodi, W., and Scheuerer, G.: Scrutinizing the $k-\epsilon$ Turbulence Model Under Adverse Pressure Gradient Conditions. *Transactions of ASME*, Vol. 108, June 1986, pp. 174-179.
11. Launder, B. E., Priddin, C. H., and Sharma, B. I.: The Calculation of Turbulent Boundary Layers of Spinning and Curved Surfaces. *J. Fluids Engr.*, 1977, pp. 231-239.
12. Rodi, W.: Influence of Buoyancy and Rotation on Equations for the Turbulent Length Scale. *Proc. 2nd Symp. Turbulent Shear Flows*, London, Imperial College, 1979, pp. 10.37-10.42.
13. Uberoi, M. S.: Equipartition of Energy and Local Isotropy in Turbulent Flows. *J. Appl. Physics*, Vol. 28, 1957, pp. 1165-1170.
14. Champagne, F. H., Harris, V. G., and Corrsin, S.: Experiments on Nearly Homogeneous Turbulent Shear Flow. *J. Fluid Mech.*, Vol. 41, Part 1, pp. 81-139, 1970.

15. Harris, V. G., Graham, J. A. H., and Corrsin, S.: Further Experiments in Nearly Homogeneous Turbulent Shear Flow. *J. Fluid Mech.*, Vol. 81, Part 4, 1977, pp. 657-687.
16. Laufer, J.: Investigation of Turbulent Flow in a Two-Dimensional Channel. NACA CR-1053, 1949.
17. Laufer, J.: The Structure of Turbulence in Fully Developed Pipe Flow. NACA TR-1174, 1954.
18. Robins, A.: The Structure and Development of a Plane Turbulent Free Jet. Ph.D. Thesis, University of London, 1971.
19. Corrsin, S., and Uberoi, M. S.: Further Experiments on the Flow and Heat Transfer in a Heated Turbulent Air Jet. NACA TN-1865, 1949.
20. Bradbury, L. J. S.: The Structure of a Self-Preserving Turbulent Plane Jet. *J. Fluid Mech.*, Vol. 23, 1965, pp. 31-64.
21. Antonia, R. A., and Bilger, R. W.: An Experimental Investigation of an Axisymmetric Jet in a Co-Flowing Air Stream. *J. Fluid Mech.*, Vol. 61, 1973, pp. 805-822.
22. Wiehardt, K., and Tillmann, W.: Wiehardt Flat Plate Flow, Flow 1400. Eds. D. E. Coles and E. A. Hirst, Proc. Computation of Turbulent Boundary Layers, AFOSR-IFP-Stanford Conference, 1968.
23. Chen, Y.-S.: A Computer Code for Three-Dimensional Incompressible Flows Using Nonorthogonal Body-Fitted Coordinate Systems. NASA CR-178818, March 1986.
24. Chen, Y.-S.: A Numerical Method for Three-Dimensional Incompressible Flows Using Nonorthogonal Body-Fitted Coordinate Systems. AIAA Paper 86-1654, 22nd Joint Propulsion Conference, June 1986.
25. Kim, S.-W., and Chen, Y.-S.: Computation of Turbulent Boundary Layer Flows with an Algebraic Stress Turbulence Model. NASA CR-178967, 1986.
26. Anderson, D. A., Tannehill, J. C., and Pletcher, R. H.: Computational Fluid Mechanics and Heat Transfer. McGraw-Hill, New York, 1984.
27. Schlichting, H.: Boundary Layer Theory. McGraw-Hill, New York, 1968.
28. Rodi, W.: The Prediction of Free Boundary Layers by Use of a Two-Equation Model of Turbulence. Ph.D. Thesis, University of London, 1972.
29. Ljuboja, M., and Rodi, W.: Calculation of Turbulent Wall Jets with an Algebraic Stress Model. *Transaction of ASME*, Vol. 102, pp. 350-356, 1980.
30. Launder, B. E.: A Generalized Algebraic Stress Transport Hypothesis. *J. AIAA*, Vol. 20, pp. 436-437, 1982.
31. Schumann, U.: Realizability of Reynolds-Stress Turbulence Models. *The Physics of Fluids*, Vol. 20, No. 5, pp. 721-725, May 1977.

32. Sloan, D. G.: Modeling of Swirling and Heterogeneous Char Combustion in Pulverized Coal Systems. Ph.D. Thesis, Brigham Young University, 1985.
33. Syed, S., and Chiappetta, L.: Finite Difference Methods for Reducing Numerical Diffusion in TEACH-Type Calculations. AIAA Paper 85-0057, AIAA 23rd Aerospace Sciences Meeting, January 1985.
34. Brondum, D. C., Bennett, J. C., Weinberg, B. C., and McDonald, H.: Numerical and Experimental Investigation of Nonswirling and Swirling Confined Jets. AIAA Paper 86-0040, AIAA 24th Aerospace Sciences Meeting, January 1986.



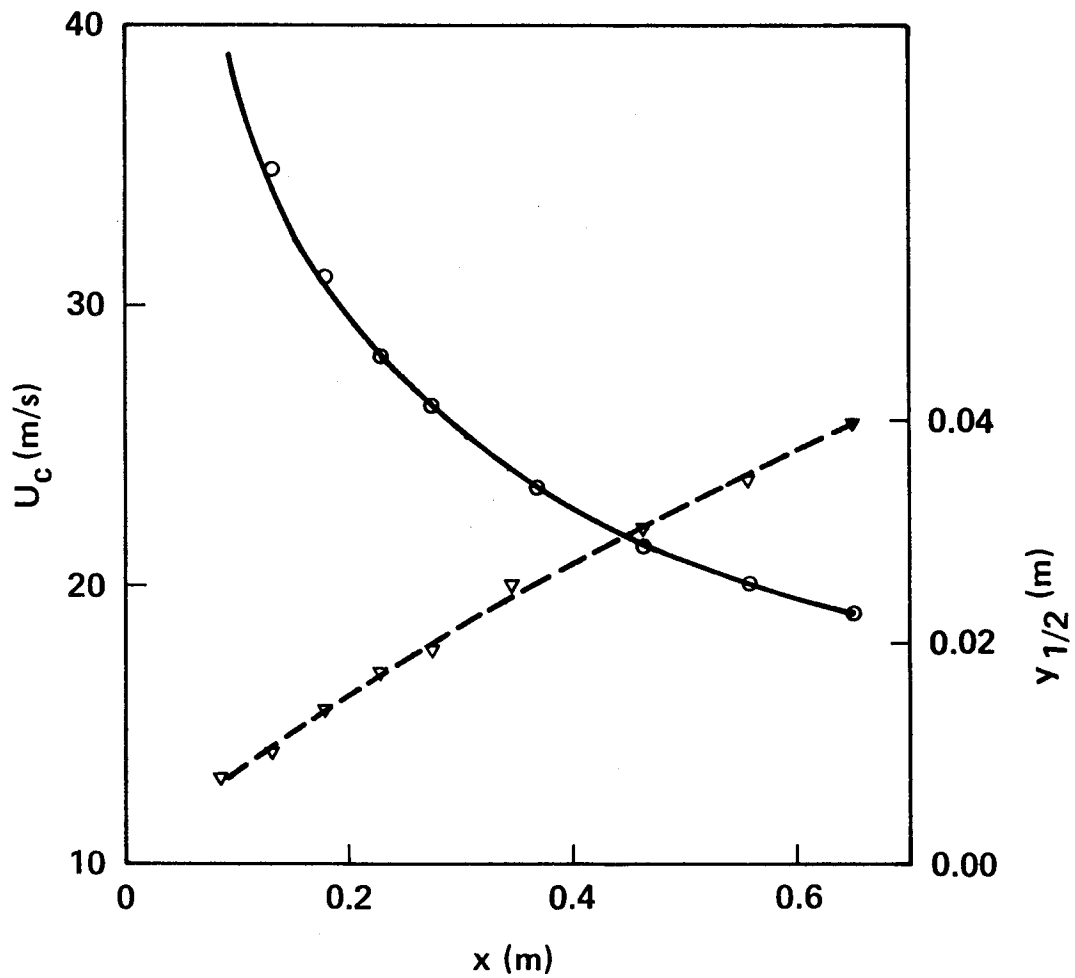
(a) FULLY DEVELOPED CHANNEL FLOW



(b) FULLY DEVELOPED PIPE FLOW

Exp't: o: velocity (u), Δ : turbulent kinetic energy (K), x : shearing stress ($-\overline{u'v'}$).
 —, ----, - - -: comp. result for u , K and $-\overline{u'v'}$, respectively.

Figure 1. Fully developed channel and pipe turbulent flows.



o: Exp't, decay of the center line velocity (u_c), ∇ : Exp't, growth of jet half width ($y_{1/2}$). —, ----: comp. result for u_c and $y_{1/2}$, respectively.

Figure 2. Plane turbulent jet exhausting into a moving stream.

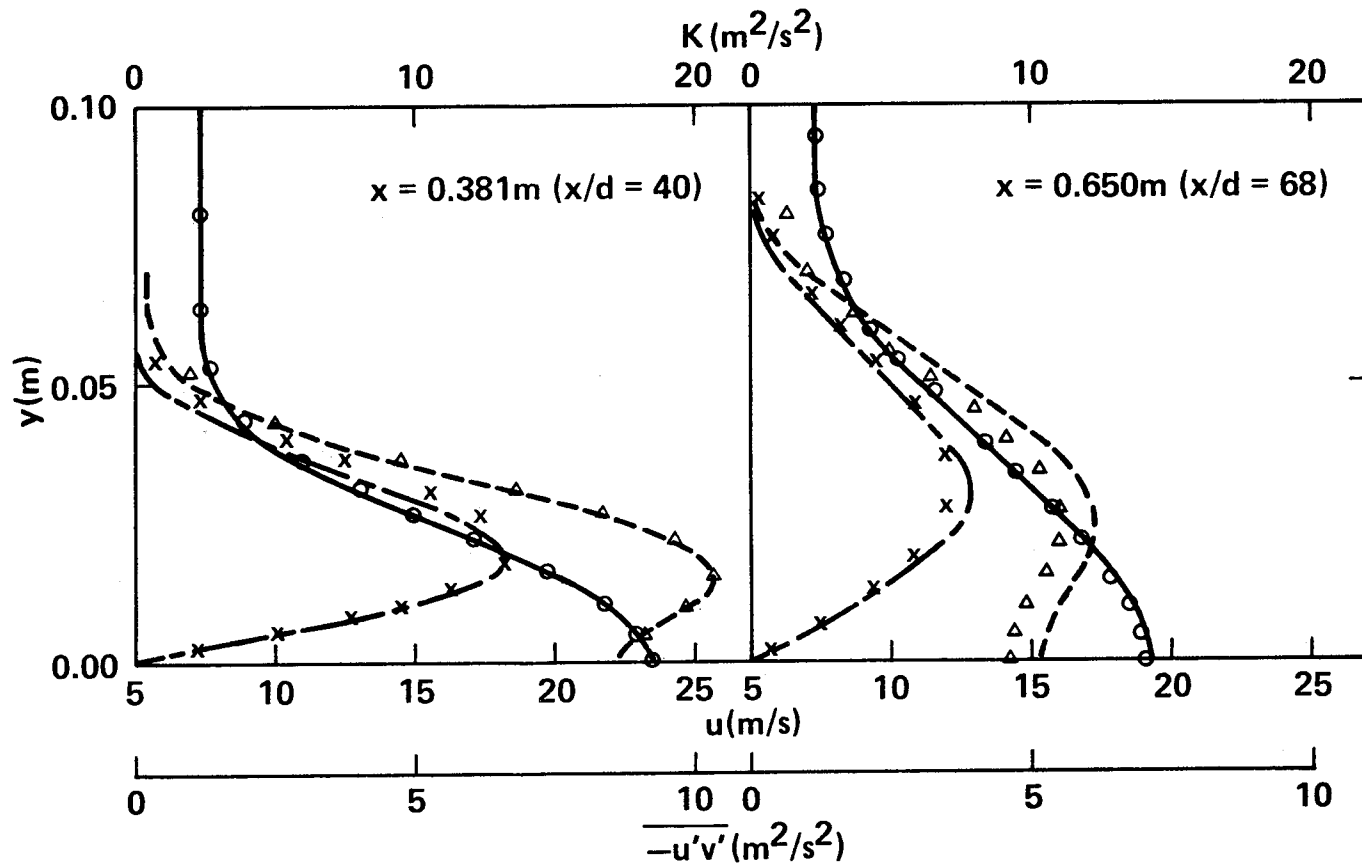


Figure 3. Plane turbulent jet exhausting into a moving stream.
(See Fig. 1 for legend.)

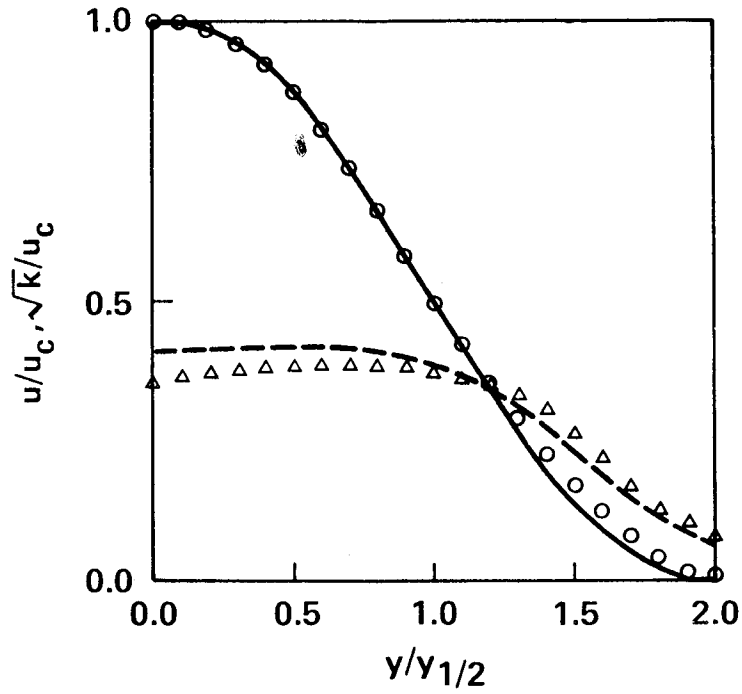


Figure 4. Axisymmetric turbulent jet exhausting into a moving stream.
(See Fig. 1 for legend.)

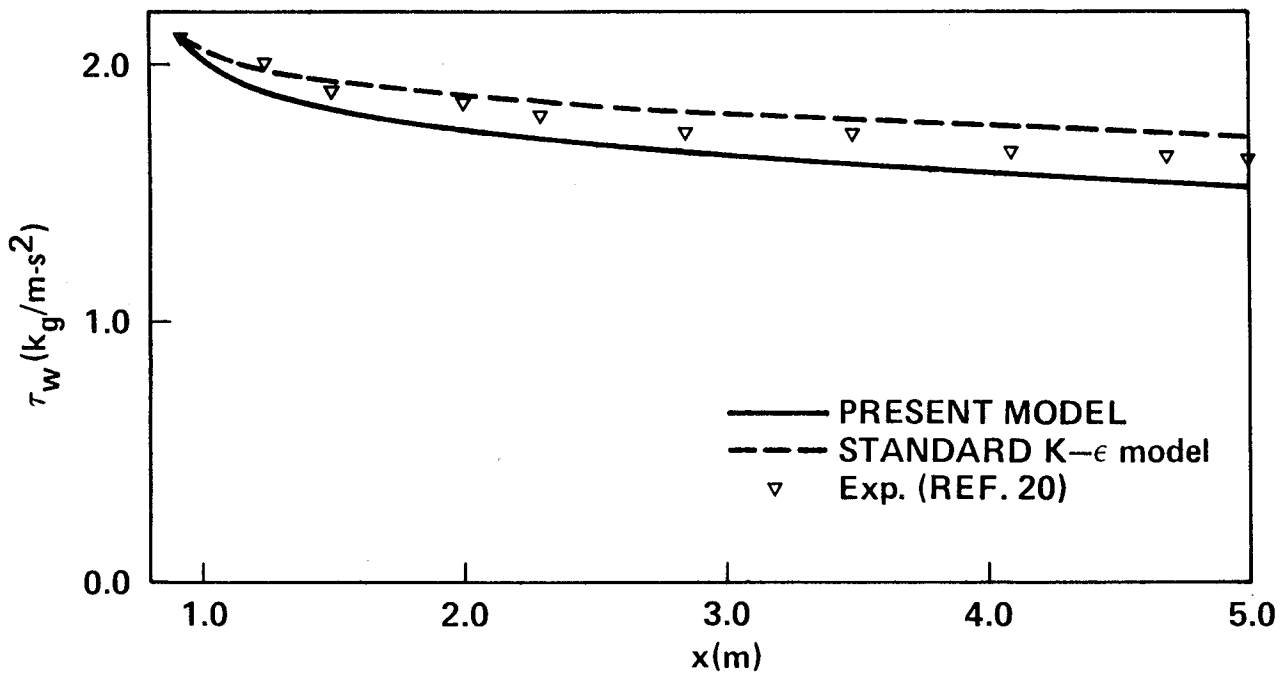


Figure 5. Wall shearing stress along a flat plate with zero pressure gradient.

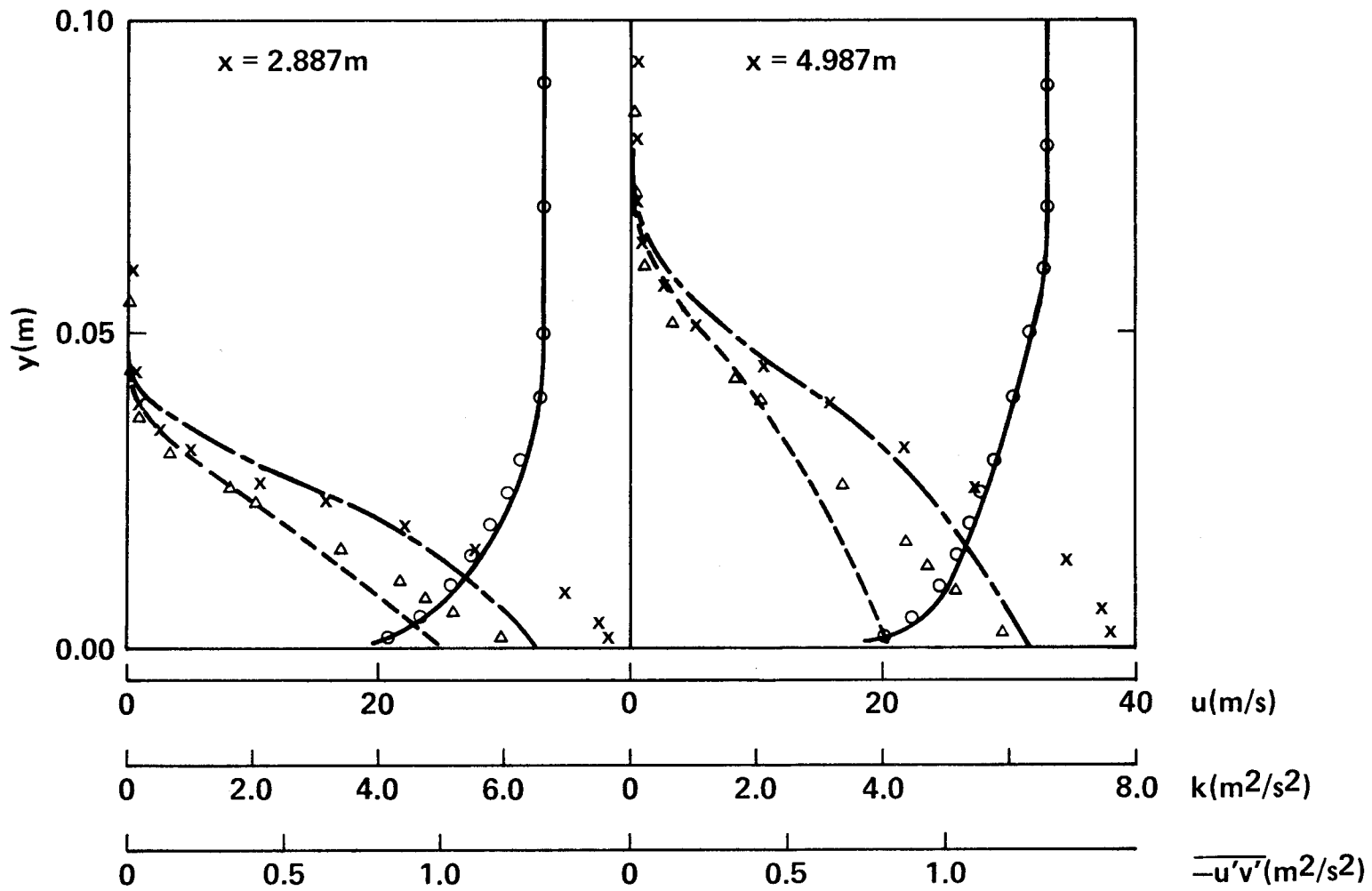


Figure 6. Flat plate turbulent boundary layer. (See Fig. 1 for legend.)

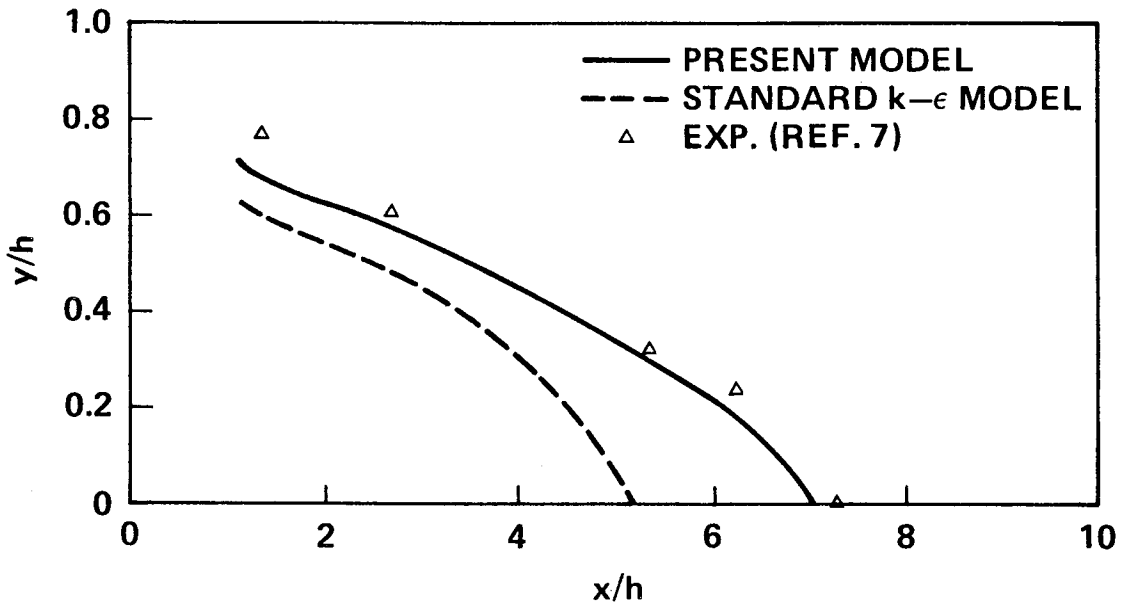


Figure 7. Locus of flow reversal downstream of a backward-facing step.

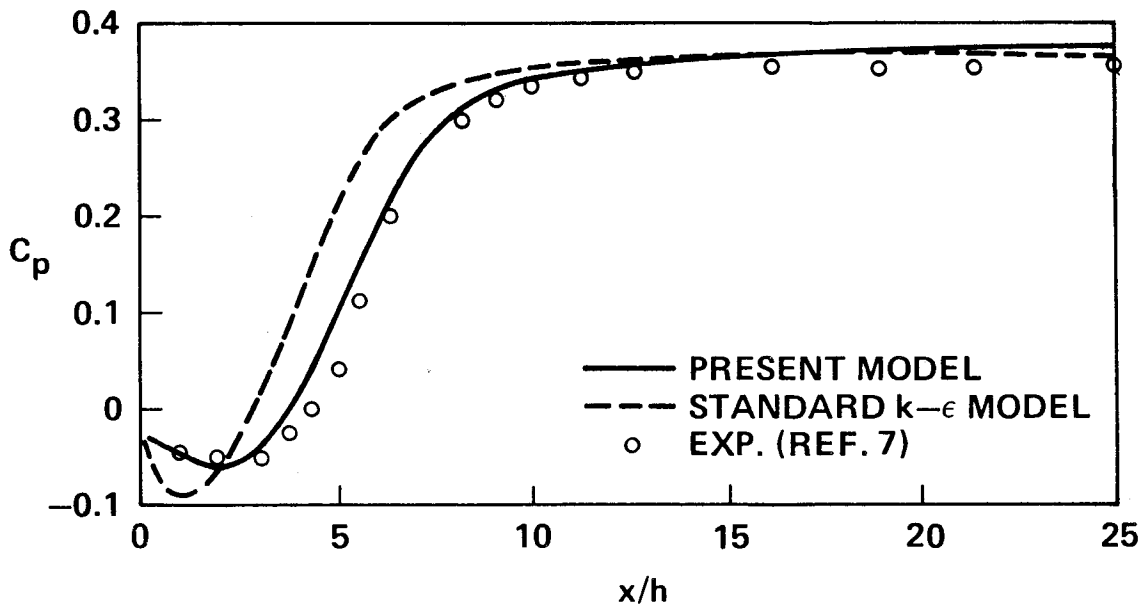


Figure 8. Static pressure coefficient distribution along the step side wall of a backward-facing step turbulent flow.

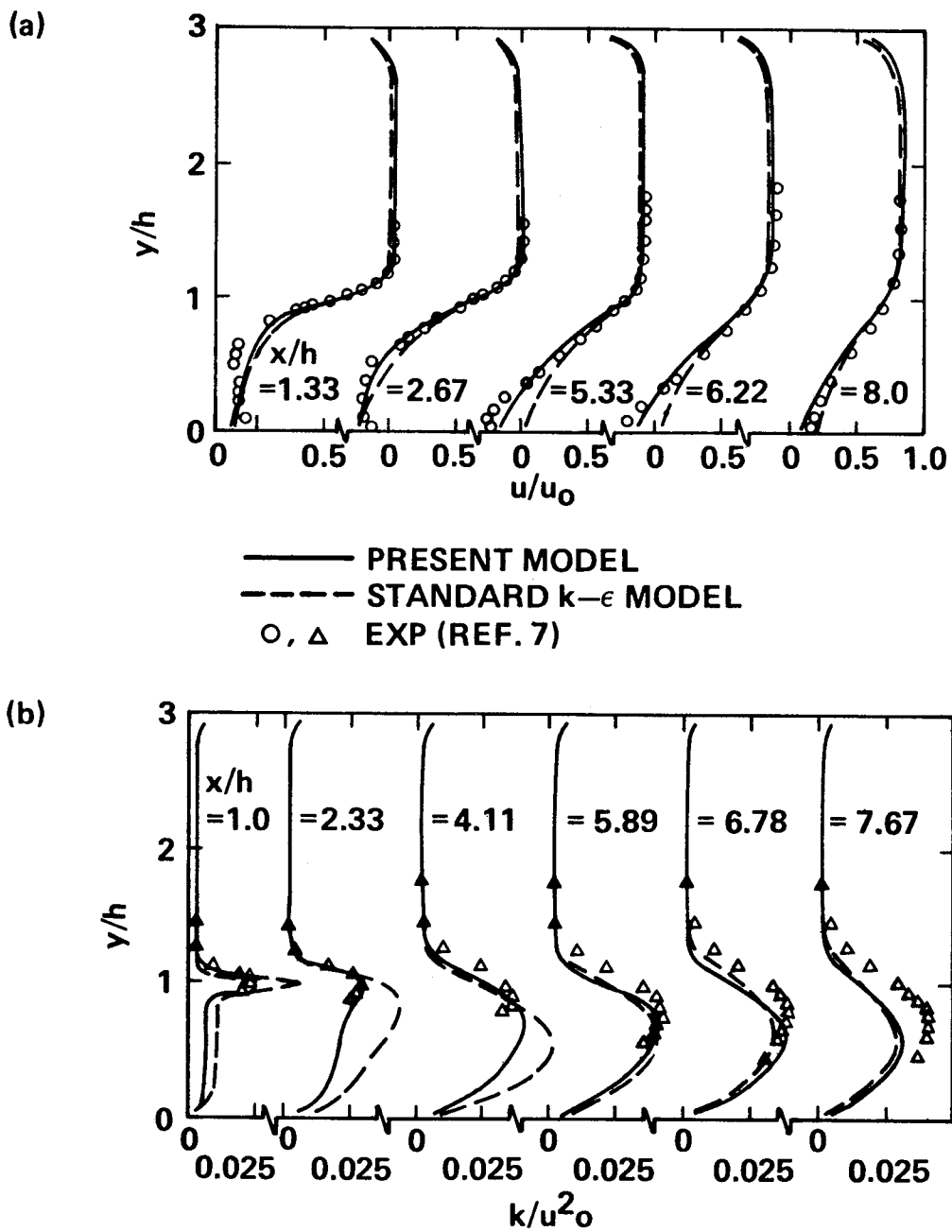


Figure 9. Mean velocity and turbulent kinetic energy profiles downstream of a backward-facing step.

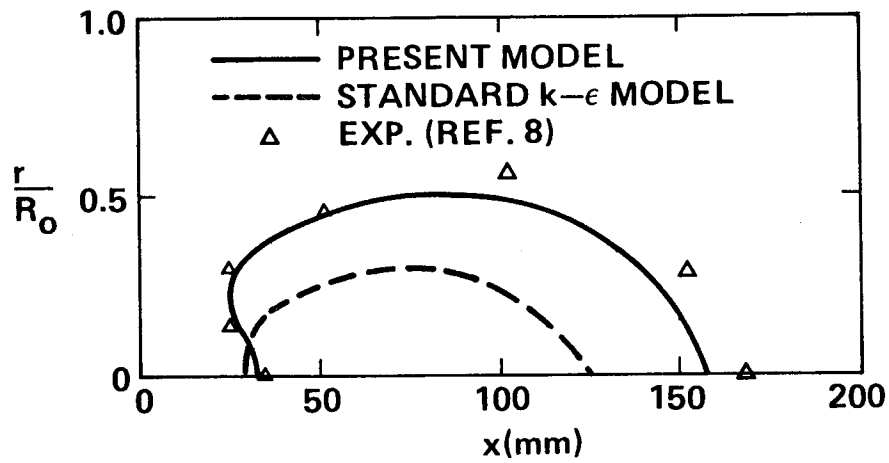


Figure 10. Envelope of the central recirculation zone of a confined swirling turbulent flow.

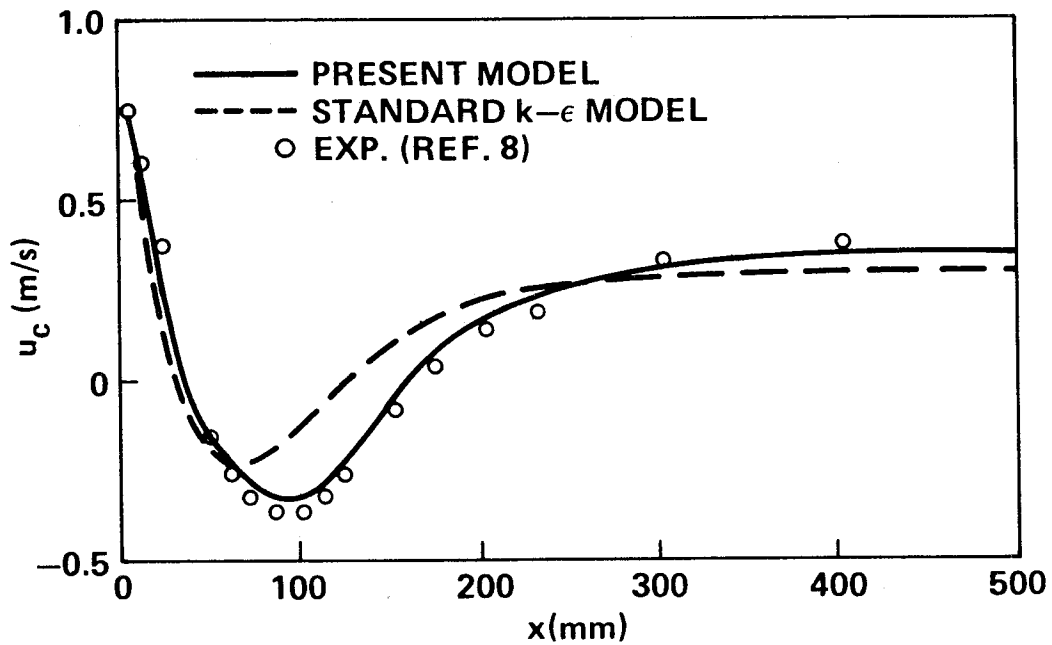


Figure 11. Center line axial velocity distribution of a confined swirling turbulent flow.

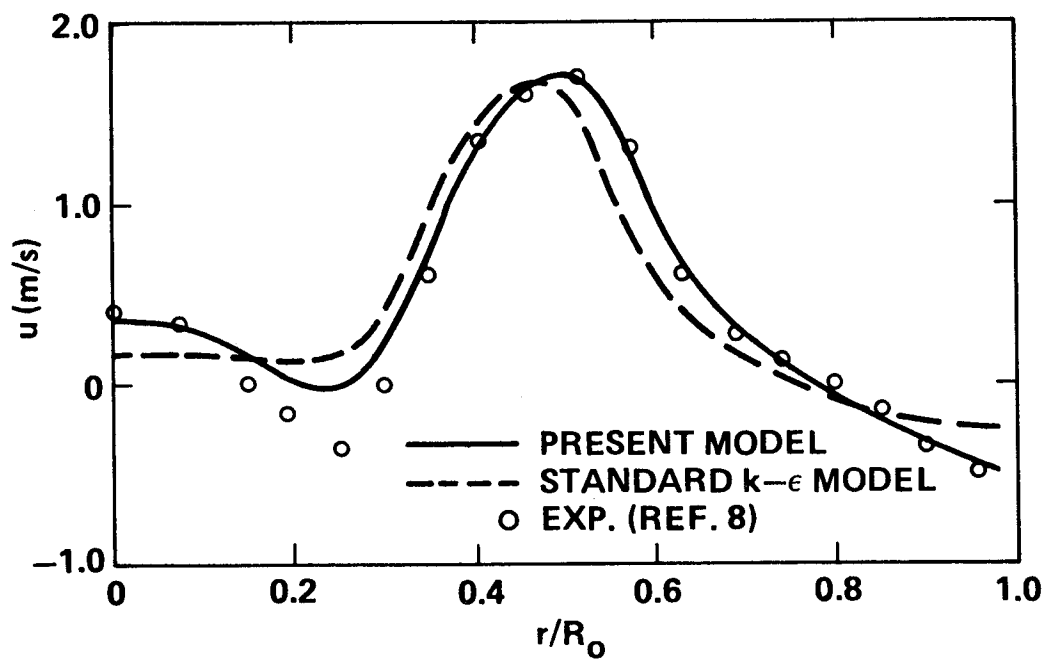


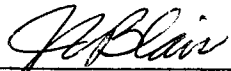
Figure 12. Radial distribution of the axial velocity at $x = 25$ mm downstream of the coaxial swirling jets.

APPROVAL

COMPUTATION OF TURBULENT FLOWS USING AN EXTENDED
k- ϵ TURBULENCE CLOSURE MODEL

By Y.-S. Chen and S.-W. Kim

The information in this report has been reviewed for technical content. Review of any information concerning Department of Defense or nuclear energy activities or programs has been made by the MSFC Security Classification Officer. This report, in its entirety, has been determined to be unclassified.



G. F. McDONOUGH

Director, Structures and Dynamics Laboratory

